Suppression of Emittance Growth Using a Shaped Cold Atom Electron and Ion Source

D. J. Thompson,[1] D. Murphy,[1] R. W. Speirs,[1] R. M. W. van Bijnen,[2] A. J. McCulloch,[1] R. E. Scholten,[1,*] and B. M. Sparkes[1]
[1]School of Physics, The University of Melbourne, Victoria 3010, Australia
[2]Eindhoven University of Technology, P.O. Box 513, 5600 MB Eindhoven, The Netherlands
(Received 20 May 2016; published 3 November 2016)

We demonstrate precise control of charged particle bunch shape with a cold atom electron and ion source to create bunches with linear and, therefore, reversible Coulomb expansion. Using ultracold charged particles enables detailed observation of space-charge effects without loss of information from thermal diffusion, unambiguously demonstrating that shaping in three dimensions can result in a marked reduction of Coulomb-driven emittance growth. We show that the emittance growth suppression is accompanied by an increase in bunch focusability and brightness, improvements necessary for the development of sources capable of coherent single-shot ultrafast electron diffraction of noncrystalline objects, with applications ranging from femtosecond chemistry to materials science and rational drug design.

DOI: 10.1103/PhysRevLett.117.193202

The elimination of Coulomb-driven emittance growth is crucial for the development of high brightness charged particle beam sources for high-energy accelerator injection [1], high-brightness x-ray sources [2], electron and ion microscopy [3,4], and ultrafast electron diffraction (UED) [5]. Single-shot UED experiments in particular require high bunch charge and short bunch duration, conditions that result in severe Coulomb-driven expansion [6,7]. For bunches with nonuniform charge density, the expansion leads to emittance growth and reduced bunch brightness and focusability. Overcoming Coulomb-driven emittance growth is, therefore, a key step towards achieving advances across fields ranging from femtosecond chemistry [8] to rational drug design [9,10] and materials science [5].

Uniformly filled three-dimensional (3D) ellipsoidal distributions, which have linear internal Coulomb fields, are ideal for the preservation of low emittance and high bunch brightness [11,12] because the bunch expansion can be fully reversed using linear electron optics. Three-dimensional ellipsoidal bunches have been created in thermal photocathode electron sources by using 2D laser pulse-shaping techniques to create "pancake" electron bunches which have a half-spherical transverse radial density profile. Provided the longitudinal profile is much narrower than the transverse radius, a pancake bunch will evolve into a uniformly filled ellipsoid under Coulomb-driven expansion [13]. The expansion properties of ellipsoidal bunches have been measured experimentally with photocathode sources [14–19], but demonstrating improved beam brightness has not been possible due to the inherently high electron temperature ($T > 1000$ K). At such temperatures, thermal diffusion quickly destroys the spatial structure of the bunch, preventing detailed observation of the effects of space-charge repulsion. High temperature also limits the initial bunch coherence, focusability and brightness of an electron source.

Cold atom electron and ion sources (CAEISs) are being developed [20–23] with the promise of orders of magnitude improvement in these key bunch metrics. The CAEIS is based on the photoionization of a laser-cooled atomic gas with two overlapping orthogonal laser beams, producing electrons and ions with low temperatures (10 K [21] and 1 mK [24], respectively), and correspondingly low emittance, high brightness, and high coherence. The initial charge distribution can be controlled by manipulating the laser beam profiles [21], allowing for full 3D shaping of the charged particle bunches at the optical resolution limit of a few micrometers [25]. Using this precise shaping ability to produce cold uniform ellipsoidal bunches is an important step towards creating a source capable of single-shot ultrafast coherent diffraction imaging of noncrystalline targets [26].

In this Letter, we describe experiments that demonstrate suppression of space-charge induced emittance growth for improved focusability and brightness, using shaped charged particle bunches from a CAEIS. Cold ions were used rather than electrons because their much lower temperature, and hence, negligible thermal diffusion, enhances the visibility of space-charge dynamics. In a CAEIS, measurements of the charge distribution for nanosecond duration ion bunches are directly analogous to picosecond electron bunches, because the heavier ion bunches disperse much more slowly than low-mass electrons within the accelerator region, retaining their high charge density and, therefore, exhibiting much stronger space-charge effects [27].

We quantify the beam expansion in terms of emittance, a measure of the phase-space volume occupied by the bunch, where low beam emittance corresponds to the desirable characteristics of high focusability and brightness. In thermal equilibrium, the transverse emittance can be defined along an axis x transverse to the beam propagation direction z, as

$$\epsilon_x = \sigma_x \sqrt{\frac{k_B T_x}{mc^2}}, \quad (1)$$

where σ_x is the root mean square (rms) beam width, k_B is the Boltzmann constant, m is the mass of the beam particles, and c is the speed of light. The axial particle temperature can be defined as $T_x = m\sigma_{v_x}^2(1 - R_{x,v_x}^2)/k_B$, where σ_{v_x} is the rms velocity in the x axis and R_{x,v_x} is the correlation coefficient measuring the linearity of the particle position x and velocity v_x phase-space profile. Nonlinear space-charge forces cause distortion of the beam phase-space profile, increasing beam emittance. The normalized transverse beam brightness $\mathcal{B}_{n\perp}$ varies as ϵ_x^{-2}; hence, a reduction in the emittance will lead to an increase in the transverse beam brightness.

Ion bunches were created via two-color, near-threshold photoionization of an ensemble of rubidium atoms cooled to a temperature of 100 μK in a magneto-optical trap (see Fig. 1). The cloud of cold atoms had a Gaussian spatial density profile with a standard deviation of 500 μm and peak density of 3.0×10^{16} atoms m^{-3}. A 780 nm wavelength laser beam was used to excite atoms from the $5S_{1/2}$ ground state to the $5P_{3/2}$ excited state for 500 ns, with a transverse intensity profile shaped by a spatial-light modulator (SLM). Beam shaping was performed with a speckle-free protocol based on iterative feedback [25]. Atoms in the excited state were coupled to the ionization continuum with a 480 nm wavelength, 5 mJ, 5 ns laser pulse propagating through the atom cloud perpendicular to the excitation beam. The ionization beam was focused to a narrow ribbon at the cold atom cloud with rms intensity widths $\sigma_z = 15$ μm along the longitudinal direction of ion propagation and $\sigma_y > 1$ mm in the axis perpendicular to both the excitation and ionization laser propagation directions. The two-color ionization process produced ion bunches that initially had a very narrow longitudinal distribution compared to the length of the accelerator region (50 mm), ensuring that the longitudinal energy spread was only a few eV. Provided the intensity of the excitation laser beam is below the saturation intensity of the $5S \rightarrow 5P$ transition, the transverse excited atomic density profile $\rho_e(r)$ is proportional to $\Omega_e(r)$, the Rabi frequency for the driven transition. Control of the bunch charge was achieved by altering the excitation laser beam power and, thus, the overall population of the intermediate state prior to ionization by the 480 nm laser. The duration of the ion bunches was determined by the 480 nm laser pulse length

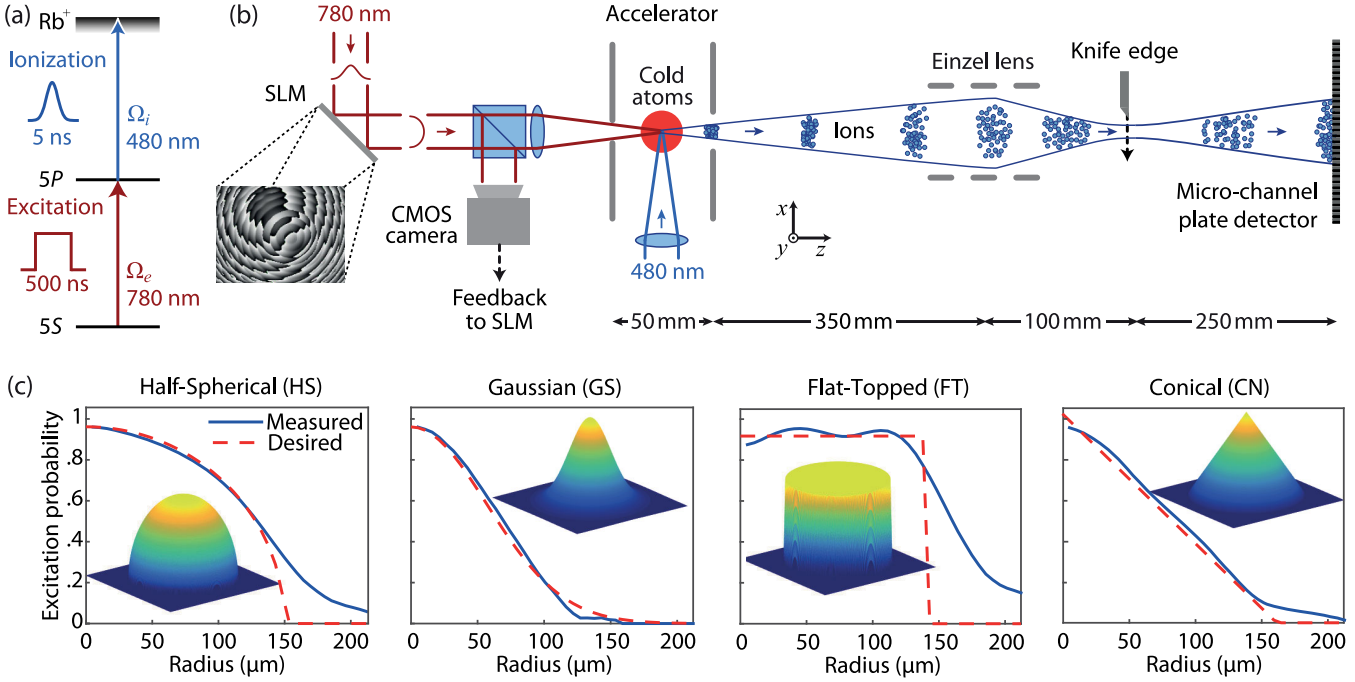

FIG. 1. (a) Two-color laser excitation scheme used to ionize laser-cooled ^{85}Rb atoms. (b) Cold atom electron and ion source with bunch shaping. The intensity profile of the excitation laser coupling the $5S$ ground state to the $5P$ intermediate state was shaped using a spatial-light modulator (SLM) with iterative feedback provided via a CMOS camera [25]. Atoms were ionized with a 5 ns pulsed blue laser, focused to a narrow ribbon perpendicular to the excitation laser. The ions were accelerated into a drift region and focused with an einzel lens. A knife edge was inserted into the bunch around the focus to determine the transverse focal spot width. Spatial bunch profiles and bunch charges were measured with a phosphor-coupled microchannel plate (MCP) detector combined with a CCD camera (not shown). (c) Measured radially averaged excitation laser profiles (solid lines) and desired profiles (dashed lines), plotted as the relative excitation probability. Insets show desired transverse bunch density profiles as shaded false-color renderings. All radial averages and density profiles are individually normalized.

(5 ns), analogous to an electron bunch duration of 13 ps [27].

To investigate the effect of transverse bunch shape on emittance growth, we studied four bunch distributions: half-spherical (HS), required to make pancake bunches; Gaussian (GS), i.e., an "unshaped" laser beam; flat-topped (FT), a uniform transverse profile with complementary application to pancake distributions [28]; and conical (CN), chosen as an example of a nonideal distribution. The excitation laser intensity profile $I_e(r) \propto \Omega_e^2$ was controlled by the SLM to create each initial transverse bunch distribution. Radial distributions of the excitation probability shown in Fig. 1(c) were calculated from each measured laser intensity profile. There was generally good agreement between the measured and desired distributions, with some loss of definition at the edges of the flat-topped and half-spherical distributions.

We initially studied the expansion of the shaped ion bunches for free propagation. Ion bunches with a range of charge densities were accelerated to 6 keV and propagated 700 mm to the detector where the transverse particle distributions were measured using a phosphor-coupled microchannel-plate (MCP) and camera. The initial radius encompassing 95% of the charge was $r_{95} = 139$ μm for all distributions, satisfying $r_{95} \gg \sigma_z$ required for the HS distribution to create a pancake bunch. Figure 2(a) shows the final transverse bunch distributions for ion numbers $N = 2.0 \times 10^3$, where there is negligible space-charge expansion, and $N = 7.1 \times 10^4$, where the growth is dominated by space-charge expansion. For higher charge, all distributions obtain a dense ring structure due to scattered 780 nm light absorbed by atoms outside the interaction region. These atoms were subsequently ionized by the 480 nm light pulse, creating a diffuse halo of electrons. The core ion bunch will expand much faster than the halo due to its higher charge density, resulting in transverse velocity bunching at the edges [27].

Bunches with linear space-charge forces undergo self-similar expansion, where the beam charge density profile is magnified by a single scaling factor. To assess the self-similarity of the CAEIS bunch expansion, we measured the transverse radii containing 50%, 75%, 90%, and 95% of the bunch charge for the different distributions at the detector. We then took the ratio of these radii to their initial values from the laser distribution to obtain the expansion factors denoted e_{50}, e_{75}, e_{90}, and e_{95} [Fig. 2(b)].

At low ion numbers, bunch expansion is mainly determined by lensing in the accelerator structure such that all shapes show approximately equal linear expansion by a factor of 20. As the ion number increases, and space-charge effects become more significant, the central radii expansion factors e_{50} and e_{75} of the GS and CN distributions increase more than the factors for the outer radii (e_{90} and e_{95}) due to the large initial central densities. The opposite behavior is true for the FT, with e_{50} and e_{75} increasing above e_{90} and

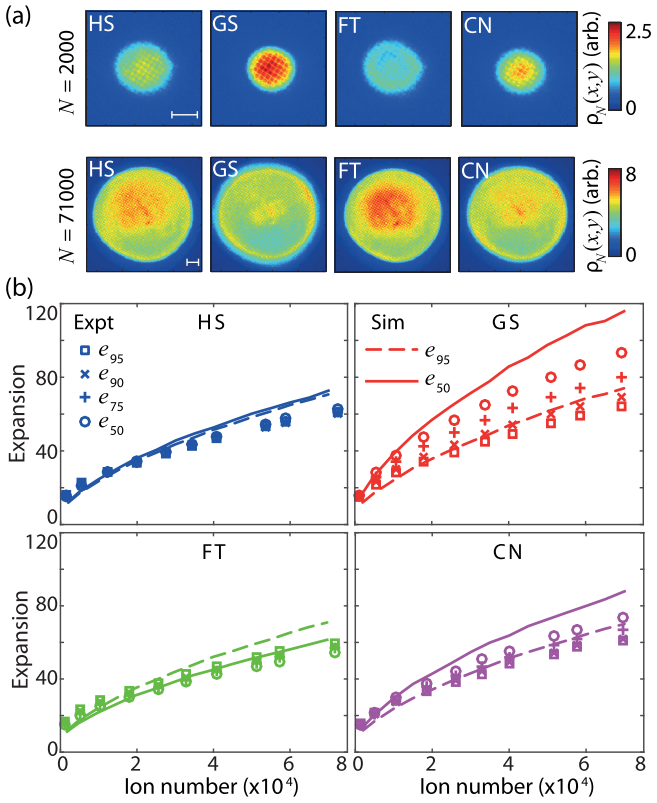

FIG. 2. (a) Experimentally measured transverse ion beam density profiles $\rho_N(x, y)$ for ion number $N = 2\,000$ and 71 000, for HS, GS, FT, and CN initial distributions (scale bar, 2 mm). (b) Radial expansion factors against ion number for each shape individually, with circle, plus, times, and square corresponding to the transverse radii containing 50%, 75%, 90%, and 95% of the bunch charge, respectively. The divergence of the expansion factors at high ion numbers indicate nonlinear space-charge forces, most prevalent in the GS and CN bunches. Simulated expansion factors e_{95} (dashed lines) and e_{50} (solid lines) for each shape are also shown. Measured radii are averaged from 100 ion bunches.

e_{95}, due to the lower initial central density. For the HS initial distribution, the expansion factors remain equal as the ion number increases, signifying linear self-similar space-charge expansion and formation of the desired uniform ellipsoid [13,29].

We simulated the acceleration, propagation, and expansion of the ion bunches using particle tracking software [30] for ideal spatial and measured temporal profiles, and an initial ion temperature of 1 mK. From these simulations, we extracted the expected expansion factors shown in Fig. 2(b). The simulations agree well with the experimental data, especially for the HS distribution. The smaller expansion of the experimental bunches at higher charge is attributed to the ions in the halo discussed earlier, which contribute to the measured ion number but not to the space-charge expansion. The greater deviation seen for the highly peaked GS and CN

distributions could also indicate saturation of the $5S \rightarrow 5P$ transition in the center.

At a beam waist, the transverse emittance [Eq. (1)] is the product of beam width and angular divergence. Measurement of the focal spot width for beams with different initial distributions, therefore, provides a measure of their relative emittance. To investigate the space-charge-induced emittance growth, an einzel lens situated 350 mm from the accelerator was used to focus the expanding bunches. The same transverse rms bunch width $\sigma_x = \sigma_y = 67\ \mu$m was used for all distributions to allow direct emittance comparison. A knife edge was scanned transversely through the propagating bunches at a range of z locations approximately 100 mm from the einzel lens. The rms width $\sigma_r(z)$ was determined from a fit of each profile to an error function (erf) [Fig. 3(a)]. The minimum focused bunch width σ_f was found from a parabolic fit of $\sigma_r(z)$ [Fig. 3(b)].

Figure 3(c) shows how σ_f varies for the different initial spatial distributions as the total ion number increases. The

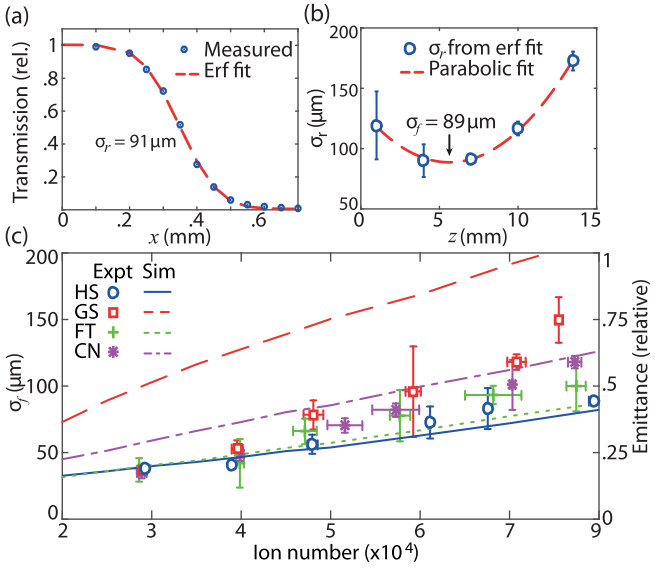

FIG. 3. (a) Example knife-edge plot of relative transmission (points) and erf fit (dashed line) to determine the transverse rms width σ_r at a given z position. (b) Example z scan of knife-edge transmission around the focus. Points indicate the knife-edge measurement and the dashed line is a weighted parabolic fit to determine the minimum rms width σ_f. Error bars are 95% confidence intervals determined from the fit in (a). (c) Experimentally measured minimum rms width (left-hand axis, points) and simulated emittance of freely expanding bunches (right-hand axis, lines) as a function of ion number for the four transverse spatial profiles: HS (blue, circles, solid line), GS (red, squares, dashed line), FT (green, crosses, dotted line), and CN (purple, stars, dashed-dotted line). Uncertainty in ion number is determined from standard deviation of ion numbers from all knife-edge measurements used to determine $\sigma_f(z)$, uncertainty in σ_f is determined from standard error of fitted parabolas in (b). Ion temperature for simulations was taken to be $T = 1$ mK.

GS and CN distributions, which demonstrated the most nonlinear growth in Fig. 2(c), show the greatest increase in emittance with bunch charge, while the linearly expanding HS distribution demonstrates the smallest increase as expected. Aperturing of the bunches in the accelerator structure limited the maximum number of ions to $N = 8 \times 10^4$, where we observe a 50% reduction in focused bunch width and, therefore, transverse emittance for the HS compared to GS distributions.

Particle tracking simulations of the free-expansion emittance for the four distributions exhibit the same behavior, though with a greater variation between the distributions. The greatest deviation is seen at low N, where space-charge expansion is negligible and bunch emittance will mostly be determined by accelerator aberrations and effects such as disorder-induced heating [31]. As N increases and space-charge dominates the emittance growth, there is much closer agreement between the experimental results and simulations, with the GS distribution showing the greatest difference. As with the free-expansion results, the discrepancies can be attributed to a combination of the formation of a ring structure, which will be more prominent for distributions created with higher peak 780 nm intensity, and saturation at the center. The separation between experimentally measured FT and HS waists is attributed to the imperfect flat-topped laser profile [Fig. 1(c)(ii)]. Nevertheless, the HS profile again matches very well with the simulations and shows that bunch shaping with a CAEIS can lead to a marked reduction in emittance growth relative to conventional Gaussian bunches.

In this Letter, we have experimentally demonstrated improvement of charged particle beam brightness through control of transverse bunch density distribution. The low temperature of the cold atom source has enabled detailed observation of space-charge effects, for the first time clearly distinguishing the variation in nonlinear growth for different initial particle distributions. For space-charge-dominated bunches with $N = 7.1 \times 10^4$ particles, a reduction in emittance growth of nearly 50% was achieved for a half-spherical rather than Gaussian transverse distribution, corresponding to a brightness increase by a factor of 4. Further improvements in beam brightness are expected if the spatial width of the pulsed blue laser beam is reduced to better satisfy the requirements for a half-spherical pancake distribution to transform into a uniformly filled ellipsoid [13].

The 5 ns ion bunches used for our demonstrations are directly analogous to ultrafast 13 ps electron bunches [27,31] with the same bunch charge. Achieving ultrafast single-shot diffraction will require much higher charge density, and much higher bunch charge such as the $N = 5 \times 10^5$ electron bunches we have previously produced with a cold atom source [32]. The effects of Coulomb-driven emittance growth will then severely limit the beam focus and brightness for unshaped Gaussian

bunches. Indeed, other cold atom sources using ultrafast electron bunches have been limited to a few hundred electrons per bunch due to the degrading effects of space charge, requiring thousands of bunches to create a satisfactory diffraction image [33]. Demonstrating the suppression of space-charge-induced emittance growth through shaping of the initial bunch profile is, therefore, a critical milestone in the development of cold electron sources, necessary for harnessing their inherent coherence, focusability, and brightness to perform single-shot ultrafast diffraction of noncrystalline targets.

B. M. S. acknowledges the support of a University of Melbourne McKenzie Fellowship. This work was supported by the Australian Research Council Discovery Project No. DP140102102.

*scholten@unimelb.edu.au

[1] S. Bernal, H. Li, T. Godlove, I. Haber, R. A. Kishek, B. Quinn, M. Reiser, M. Walter, Y. Zou, and P. G. O'Shea, Phys. Plasmas **11**, 2907 (2004).
[2] R. W. Schoenlein, W. P. Leemans, A. H. Chin, P. Volfbeyn, T. E. Glover, P. Balling, M. Zolotorev, K. Kim, S. Chattopadhyay, and C. V. Shank, Science **274**, 236 (1996).
[3] N. M. Buckanie, J. Göhre, P. Zhou, D. von der Linde, M. Horn-von Hoegen, and F. J. Meyer zu Heringdorf, J. Phys. Condens. Matter **21**, 314003 (2009).
[4] J. Orloff, Rev. Sci. Instrum. **64**, 1105 (1993).
[5] B. J. Siwick, J. R. Dwyer, R. E. Jordan, and R. J. D. Miller, Science **302**, 1382 (2003).
[6] Z. Tao, H. Zhang, P. M. Duxbury, M. Berz, and C.-Y. Ruan, J. Appl. Phys. **111**, 044316 (2012).
[7] F. O. Kirchner, A. Gliserin, F. Krausz, and P. Baum, Nat. Photonics **8**, 52 (2014).
[8] J. C. Williamson, J. Cao, H. Ihee, H. Frey, and A. H. Zewail, Nature (London) **386**, 159 (1997).
[9] L. W. Hardy, J. S. Finer-Moore, W. R. Montfort, M. O. Jones, D. V. Santi, and R. M. Stroud, Science **235**, 448 (1987).
[10] I. D. Kuntz, Science **257**, 1078 (1992).
[11] O. D. Kellogg, *Foundations of Potential Theory* (Springer-Verlag, Berlin, 1929).
[12] I. M. Kapchinskij and V. V. Vladimirskij, in *Proceedings of the International Conference on High Energy Accelerators* (CERN, Geneva, 1959), p. 274.
[13] O. J. Luiten, S. B. van der Geer, M. J. de Loos, F. B. Kiewiet, and M. J. van der Wiel, Phys. Rev. Lett. **93**, 094802 (2004).
[14] P. Musumeci, J. T. Moody, R. J. England, J. B. Rosenzweig, and T. Tran, Phys. Rev. Lett. **100**, 244801 (2008).
[15] J. T. Moody, P. Musumeci, M. S. Gutierrez, J. B. Rosenzweig, and C. M. Scoby, Phys. Rev. ST Accel. Beams **12**, 070704 (2009).
[16] Y. Li, S. Chemerisov, and B. Shen, New J. Phys. **12**, 123011 (2010).
[17] B. O'Shea, J. B. Rosenzweig, G. Asova, J. Bähr, M. Hänel, Y. Ivanisenko, M. Khojoyan, M. Krasilnikov, L. Staykov, F. Stephan *et al.*, Phys. Rev. ST Accel. Beams **14**, 012801 (2011).
[18] R. K. Li, K. G. Roberts, C. M. Scoby, H. To, and P. Musumeci, Phys. Rev. ST Accel. Beams **15**, 090702 (2012).
[19] P. Piot, Y. E. Sun, T. J. Maxwell, J. Ruan, E. Secchi, and J. C. T. Thangaraj, Phys. Rev. ST Accel. Beams **16**, 010102 (2013).
[20] B. J. Claessens, S. B. van der Geer, G. Taban, E. J. D. Vredenbregt, and O. J. Luiten, Phys. Rev. Lett. **95**, 164801 (2005).
[21] A. J. McCulloch, D. V. Sheludko, S. D. Saliba, S. C. Bell, M. Junker, K. A. Nugent, and R. E. Scholten, Nat. Phys. **7**, 785 (2011).
[22] A. J. McCulloch, D. V. Sheludko, M. Junker, and R. E. Scholten, Nat. Commun. **4**, 1692 (2013).
[23] W. J. Engelen, M. A. van der Heijden, D. J. Bakker, E. J. D. Vredenbregt, and O. J. Luiten, Nat. Commun. **4**, 1693 (2013).
[24] N. Debernardi, M. P. Reijnders, W. J. Engelen, T. T. J. Clevis, P. H. A. Mutsaers, O. J. Luiten, and E. J. D. Vredenbregt, J. Appl. Phys. **110**, 024501 (2011).
[25] R. M. W. van Bijnen, C. Ravensbergen, D. J. Bakker, G. J. Dijk, S. J. J. M. F. Kokkelmans, and E. J. D. Vredenbregt, New J. Phys. **17**, 023045 (2015).
[26] T. van Oudheusden, E. F. de Jong, S. B. van der Geer, W. P. E. M. Op't Root, O. J. Luiten, and B. J. Siwick, J. Appl. Phys. **102**, 093501 (2007).
[27] D. Murphy, R. W. Speirs, D. V. Sheludko, C. T. Putkunz, A. J. McCulloch, B. M. Sparkes, and R. E. Scholten, Nat. Commun. **5**, 4489 (2014).
[28] S. B. Van der Geer, M. J. De Loos, and O. J. Luiten, in *European Particle Accelerator Conference: Proceedings* (Genoa, Italy, 2008), Vol. 8, p. 151.
[29] L. Serafini, AIP Conf. Proc. **413**, 321 (1997).
[30] http://www.pulsar.nl/gpt/.
[31] D. Murphy, R. E. Scholten, and B. M. Sparkes, Phys. Rev. Lett. **115**, 214802 (2015).
[32] R. W. Speirs, C. T. Putkunz, A. J. McCulloch, K. A. Nugent, B. M. Sparkes, and R. E. Scholten, J. Phys. B **48**, 214002 (2015).
[33] M. W. van Mourik, W. J. Engelen, E. J. D. Vredenbregt, and O. J. Luiten, Struct. Dyn. **1**, 034302 (2014).